Effects of Varied Propellant Compositions on the Ion Energy Distributions in Hollow Cathodes

IEPC-2007-174

Presented at the 30th International Electric Propulsion Conference, Florence, Italy
September 17-20, 2007

JoHanna N. Przybylowski*
California Institute of Technology, Pasadena, CA, 91125

James E. Polk†
Jet Propulsion Laboratory, Pasadena, CA, 91109

Joseph E. Shepherd‡ and Angela M. Capece§
California Institute of Technology, Pasadena, CA, 91125

Radial ion energy distributions in a hollow cathode discharge were gathered via an electrostatic energy analyzer mounted 90° off of the cathode axis pointing immediately downstream of the cathode orifice for a propellant mixture of xenon and krypton. Consistent with previous studies using xenon propellant, ions with energies much greater than the potential difference between the anode and the cathode were detected. Due to the inherent variability of the discharge, the impact of small percentages of krypton on the operation was unclear. At many combinations of flow rate and discharge current, the high-energy ion content tended to increase as the amount of krypton increased. Unfortunately, it is unclear whether the alteration in the high-energy ion distribution indicates preferential acceleration of krypton or whether it reflects different operational characteristics of the discharge. The variability of discharge operation and the lack of clear trends in the data argue for further experimentation. Analysis of oscillations in the discharge voltage revealed that the total current collected and the average energy of each high-energy ion distribution are shifted-exponential functions of the peak-to-peak fluctuations in the discharge voltage. The radial high-energy content and the functional relationship on peak-to-peak fluctuations of the discharge voltage suggest a wave acceleration mechanism.

I. Introduction

THE successful performance of the NSTAR ion thruster in the Deep Space 1 technology demonstration mission and of the flight spare thruster in a 30,352 hour ground test has demonstrated the viability of electric propulsion for deep space missions; however, the long thrust times for these missions place great demands on component reliability. Erosion of the hollow cathode assembly, a major life-limiting component in electric propulsion systems, remains a serious concern for longer duration missions. High energy ion bombardment is considered the primary source of cathode keeper electrode and orifice erosion in electrostatic thrusters. While cathode erosion has been studied for many years, the mechanisms responsible for high-energy ion production and acceleration toward the cathode assembly remain unexplained. Hollow cathode discharges also generate flows of high-energy ions outward from the cathode assembly, which in some configurations can lead to erosion of downstream thruster components. The discharge region of hollow cathodes consists of

*Graduate Student, GALCIT, johannap@caltech.edu
†Section Staff, Thermal and Propulsion Engineering Section, James.E.Polk@jpl.nasa.gov
‡Professor of Aeronautics and Mechanical Engineering, GALCIT, joseph.e.shepherd@caltech.edu
§Graduate Student, GALCIT, capece@caltech.edu

non-homogeneous plasma with complex geometry and an applied magnetic field. Due to its complexity, these discharges operate in a poorly understood realm of plasma physics. Thus, observation and characterization of the ion-acceleration mechanisms will shed light on the underlying physics.

The present investigation aims to probe this unexplained high-energy ion phenomenon further by examining the ion energy distributions produced with different propellant compositions. Radial ion energy distributions are gathered via an electrostatic energy analyzer mounted 90° off of the cathode axis pointing immediately downstream of the cathode orifice. A cylindrical anode surrounding the cathode assembly forms the discharge chamber. An earlier study preliminary characterized the high-energy ion content for this configuration using both pure xenon and pure krypton propellants. This study begins to examine ion distributions obtained using a mixture of xenon and krypton. In particular, the percentage of krypton in the mixture is varied to examine the impact on the discharge operation and on the high-energy ion content. In addition to serving as a means to probe the discharge for clues to the acceleration mechanisms using existing energy analysis instruments, the data will guide the design of subsequent experiments using energy and mass analysis instrumentation to potentially discriminate between acceleration mechanisms. Oscillations of the discharge voltage are monitored to examine possible correlations with the production of high-energy ions. These and future data will be used to discriminate among current theories and guide the development of new theories. Prior experimental evidence and current theories are reviewed before addressing the details of the present study.

II. Overview of Numerical Simulations and Experimental Observations Of Cathode Erosion and High-Energy Ions

This study is motivated by two experimental observations. First, erosion of the hollow cathode assembly and engine components located downstream of the cathode, which results from sputtering by high-energy ion bombardment, has been observed in a number of experiments.[1,2] Second, ion populations with energies much greater than the discharge voltage were observed flowing from the vicinity of the cathode orifice in several subsequent investigations.[3–8]

A dramatic example of hollow cathode component erosion was observed during the 30,352 hour Extended Life Test (ELT) of the NSTAR thruster. The orifice plate of the keeper electrode, which surrounds the cathode tube, had eroded to fully expose the heater and orifice plate after only 15,000 hours of operation. When the ELT was voluntarily terminated at 30,352 hours, the cathode heater and orifice plate, which had been exposed by the loss of the keeper orifice plate, were beginning to erode.[1] The keeper electrode normally floats about 3.5-5 V above cathode potential, but a short between the cathode keeper and the cathode had caused the keeper voltage to drop to 0.4V. This short increased the potential between the plasma and the electrode and accelerated the erosion observed in the ELT. However, based on subsequent erosion rate measurement, Kolasinski and Polk predicted that even without a short over 50% of the keeper plate would be gone after 15,617 hours of operation.[9] These erosion rates are difficult to explain based on published sputter yields and ion energies associated with acceleration through the measured steady-state potential difference between the plasma and the surface.

During a 5,024 hour life test of a 6.35mm diameter hollow cathode run at a discharge current of 25A, Brophy and Garner noted a substantial amount of sputter erosion. Sputtering was unexpected since the discharge voltage ranged from 15-20V and the thresholds for xenon ions sputtering tantalum and molybdenum are 30V and 27V, respectively. In addition, they noted cone formations on the anode indicative of simultaneous deposition and sputtering, thus implying that the ions are energetic enough to sputter materials at anode potential. A cathode jet phenomenon was used to explain the existence of high-energy ions downstream of the cathode.[2]

Using prior baffle erosion data, Latham et al. found a relationship between the normalized erosion rate, which was defined as the equivalent erosion rate for xenon on tantalum, and the square of the current to be the most significant correlation with discharge parameters. In addition, they used a retarding potential analyzer (RPA) mounted at the center of the baffle to record the axial energy distribution, finding a significant number of ions having energies in excess of the keeper potential. At lower flow rates the structure of the distribution was more complex and contained more high-energy ions.[3]

There is no existing model which quantitatively predicts the distribution of ions with energies significantly in excess of the discharge voltage. However, these high energy ion distributions have been observed in the plume of hollow cathodes for many years. Williams and Wilbur used an RPA to measure the ion energy

content in the discharge of a hollow cathode-based plasma contactor emitting electrons; they also measured the plasma potential profiles, plasma densities, electron energy distributions and plasma noise levels. They postulated that the high rate of ionization between electrons and atoms flowing from the cathode orifice results in a region of high positive space charge and a high positive potential, from which ions expand radially.[4]

Using an electrostatic energy analyzer and an NSTAR prototype discharge chamber, Farnell and Williams measured ion energy distributions along the cathode centerline and at angles up to 30° off axis. They found high energy ion groups that were clearly distinguishable from the discharge ion group, which had energies near the anode potential.[5]

Kameyama and Wilbur used an electrostatic energy analyzer positioned downstream of the cathode to investigate the effects of discharge conditions on the high energy ion characteristics. Their configuration utilized a cylindrical anode and a hollow cathode constructed from 6.4mm diameter tantalum tubes with 1.6mm thick thoriated tungsten orifice plates. They tested two cathodes: one with a straight channel and one with a 16° chamfer, both having a minimum, upstream orifice diameter of 0.71mm. All distribution functions included high-energy ions. In addition, by representing spectrum as a sum of several Gaussian distributions, Kameyama and Wilbur tracked the effects of discharge conditions on high-energy ion characteristics.[6]

With an RPA positioned on-axis and 90° off-axis, Goebel[7] and Jameson[8] measured ion energy profiles at various throttle conditions for the NSTAR and NEXIS hollow cathode and chamber configurations. They detected both low-energy and high-energy components in the radial distributions, but essentially no ions with energies greater than 35V in the axial direction. In addition, measurements of plasma potential and density obtained with fast miniature scanning probes show large-amplitude oscillations with frequencies between 50kHz and 1 MHz, leading to the conjecture that the oscillations are either predator-prey modes or turbulent ion acoustic waves. By modifying the keeper to reduce the plasma oscillations, they were able to also reduce the high-energy ion content in the radial distribution.

Goebel reported peaks in the oscillating plasma potential measured near the cathode assembly with the radial scanning emissive probes of greater than 45V for an NSTAR cathode running at a discharge current of 13.1A and a voltage of 25.2V.[7] Using the experimental potential spectrum (instead of the average plasma potential) and ion densities measured in the experiment or calculated from numerical models results in calculated keeper orifice plate erosion rates that are consistent with the measured values. High-energy ions created at these peak potentials may explain the keeper erosion, but at the same operating conditions, the RPA traces indicated ions with energies as high as 90V directed radially outward from the cathode.

Over the past few years, modeling efforts have improved in their prediction of plasma parameters within hollow cathodes and in the cathode plume region. Mikellides et al. have demonstrated that classical resistivity is insufficient to explain experimental results; in addition, classical transport and Ohm's law also predict exceedingly high electron-ion relative drift speeds compared to the electron thermal speed, which would excite streaming instabilities in the plume.[10] Numerical simulations also indicated the necessity of ion heating since the assumption of cold ions fails to match experimental observations of plasma potential either qualitatively or quantitatively.[11] Incorporation of anomalous resistivity substantially improved agreement between the model predictions and experimental observations of average plasma potential; however, the source of the anomalous resistivity is not well understood and the numerical models cannot yet calculate the magnitude of potential oscillations.[11] The high electron-ion drift and the ion heating in the near-plume plasma are suggestive of ion acoustic turbulence, which could also explain the high frequency plasma fluctuations observed by Goebel et al.[7] However, previously established theories on ion acoustic turbulence can only reproduce the bulk behavior of the plasma properties.[11] Instabilities can also be generated by inhomogeneity or the presence of a magnetic field. Thus, while ion acoustic instabilities are a candidate mechanism for the additional resistivity, they are only one of many possible wave acceleration mechanisms.

Experimental observations record both unexpected erosion rates and unexplained high-energy ions. These two phenomena are closely connected: higher energy ions result in a higher sputtering rate. Thus, the motivation to understand the mechanisms responsible is two-fold; to gain insight into a complex realm of plasma physics and to remove or reduce the conditions leading to erosion.

III. Theoretical Overview of Proposed Ion Acceleration Mechanisms

The proposed mechanisms can be grouped into three main categories: electrostatic acceleration, magneto-gas dynamic acceleration by JxB forces in the orifice, and wave acceleration processes. These main categories

can be further subdivided. Both electrostatic acceleration by DC potential structures downstream of the cathode orifice and electrostatic acceleration by time-varying electric fields in the near-cathode plume have been considered. In addition, charge exchange collisions might supplement the electrostatic acceleration mechanism. Finally, while the mechanism for ion acceleration in the presence of a wave is unique, the wave type is not unique. Ion acoustic waves have been considered likely candidates; however, numerous types of oscillations and waves can be excited in a plasma, including those arising from inhomogeneity and from an applied magnetic field.

The rudimentary explanation for high ion energies is electrostatic acceleration through a potential difference. Using laser-induced fluorescence to measure erosion rates and plasma ion velocity vectors in the vicinity downstream of the discharge cathode in a 30cm ion engine, Williams et al. concluded that a potential hill accelerates ions toward the cathode, causing keeper erosion.[12] However, radial plasma potential distributions measured by Goebel et al.[7] and Jameson[8] indicate a DC potential trough along the centerline of the discharge, rising to a few volts above the anode potential near the anode. Regardless of the potential structure, the energy after acceleration depends on the total voltage difference since $E = q\Delta V$. Thus, singly ionized xenon detected at 100eV would need to have experienced a 100V potential difference; similarly, doubly ionized xenon detected at 100eV would need to have experienced a 50V potential difference. Measurements of plasma potential indicate maximum time-averaged voltage differences that are only slightly larger than the discharge voltage.[7] Therefore, it is unlikely that the mechanism for high-energy ion production is an electrostatic acceleration by DC potential structures. However, the discharge plasma potential oscillations measured by Goebel et al. had amplitudes about twice the average discharge voltage, large enough to account for high energy ions accelerated through the potential gap between the oscillation peak and cathode potential.

The importance of charge-exchange collisions in the hollow cathode discharge has also been identified. Rovey, Gallimore and Herman proposed charge exchange as a mechanism protecting the cathode assembly from axial ion bombardment and subsequent sputter erosion.[13] Katz et al. presented a hypothesis based on a double-charge-exchange process to explain the generation of high-energy ions observed radially from the cathode centerline.[14] This mechanism requires the neutralization of ions created in a high potential region after they have been radially accelerated into the potential trough and then the re-ionization of these fast neutrals after they have passed through the trough, allowing them to be accelerated through the discharge potential a second time as they fall into the detector at ground potential as illustrated in Fig. 1. Since after the first charge exchange, the potential gradient no longer influences the neutral particle, it maintains the kinetic energy gained from accelerating down the potential trough. After the second charge exchange, or re-ionization, the particle has both kinetic and potential energy contributing to the high energy measured at ground potential. Simplified numerical simulations support this hypothesis; however, they also indicate that the high-energy ions produced in this method are unlikely to cause the observed cathode assembly erosion because of their low density and mainly radial motion.

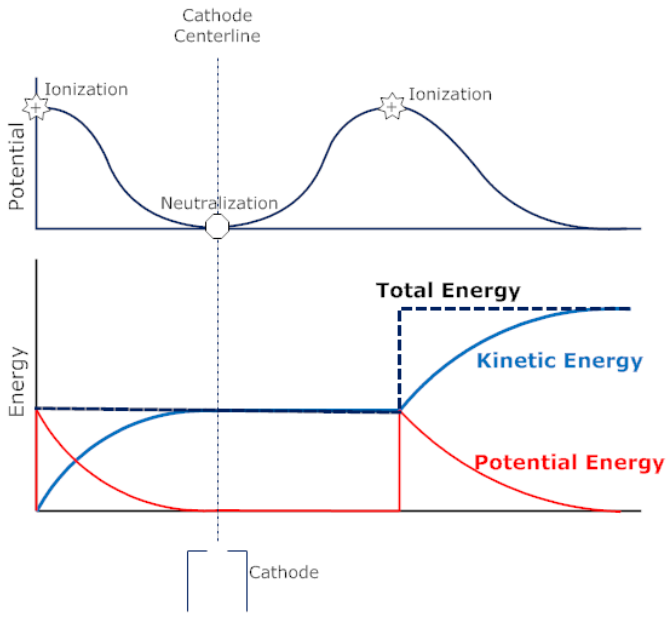

Figure 1. Diagram of proposed charge exchange mechanism. The upper curve represents a hypothetical potential distribution measured radially from the cathode centerline. The lower curve indicates the potential, kinetic and total energy of the particle. The atom is ionized at the peak in the potential and accelerated through the potential gradient, thereby increasing kinetic energy. Near the trough the ion is neutralized, resulting in a fast neutral which continues moving radially. At the second peak, the fast neutral is re-ionized and accelerated through the potential gradient toward the detector.

Based on an observed correlation between normalized baffle erosion rates and the square of the current density in the cathode orifice, Latham et al. proposed an MHD-type mechanism for ion acceleration. Since the early 1960's authors have discussed the MHD arc-pumping model and the axial velocity dependence on the square of the current.[3] Jahn demonstrates that thrust is proportional to the square of the current in a continuum model and in a particle model of the magnetoplasmadynamic arc without an applied magnetic field.[15] An applied, poloidal magnetic field introduces a swirl and an additional term contributing to the thrust. The relative significance of the terms contributing to thrust depends on the relative strengths of the induced and applied magnetic fields. While gas dynamic acceleration by JxB forces in the orifice may contribute to the production of high energy ions observed axially, it cannot account for observations of high energy ions in the radial direction. In the existing radial observations, the probe observes the vicinity immediately downstream of the cathode orifice. Since the JxB acceleration corresponds to a pinching phenomenon in the orifice, a region of high current density, there is a radial equilibrium where the pressure gradient balances the radial component of the JxB force.

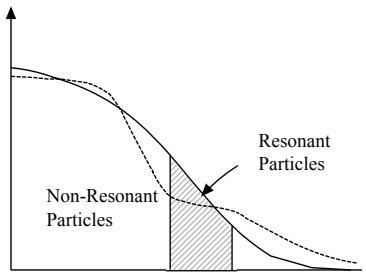

Figure 2. Sketch of the impact of a wave on a distribution function in quasi-linear plasma theory. The distribution of both the resonant particles and the non-resonant particles plateaus, with the energy of the resonant particles increasing as the wave is damped and the energy of the non-resonant particles decreases.

The theory of large amplitude waves in plasmas is complex and is still under development. An extension of the Laudau model of plasma waves to the quasi-linear theory demonstrates how plasma waves alter the equilibrium velocity distribution. For a mathematical derivation, the reader is directed to the extensive literature on quasi-linear theory starting from the early 1960s. A conceptual overview, which is appropriate for this paper, begins by considering the resonant particles. These are particles which appear trapped in the frame of the moving wave. While the total number of resonant particles is conserved, the resonant particle energy is exchanged with the wave energy. Thus, as the number of slower particles decreases, the number of faster particles must increase, creating a plateau in the distribution function for resonant particles. Energy exchange also occurs between the wave and non-resonant particles such that the non-resonant particles appear to become cooler. Thus, as the wave damps, the energy from both the non-resonant particles and the wave is transferred to the resonant particles. Fig. 2 indicates a conceptual sketch of the equilibrium distribution before the interaction with the wave and after the interaction.

IV. Experimental Apparatus

A schematic drawing experimental apparatus is shown in Fig. 3. The electrostatic analyzer (ESA) is positioned to observe ions emerging radially from the region immediately downstream of the cathode orifice. The following sections describe the cathode and anode, the flow system, the ESA, and the testing facility.

A. Cathode and Anode Assembly

A schematic drawing and a photograph of the laboratory cathode used in these experiments is shown in Fig. 4. The outer tube diameter is 6.35mm; the orifice diameter and thickness are 2.25mm and 1.5mm, respectively. The primary electron emitter had an inner diameter of 3.8mm and is a porous refractory metal insert impregnated with a barium-containing compound. A swaged coaxial heater wrapped around the downstream end of the cathode was used to condition the emitter and to preheat it prior to ignition. Radiation shielding was wrapped around the heater coil to improve the heater efficiency. The upstream end of the cathode tube is welded to a flange which is bolted to a fixture that supplies the xenon and krypton propellant.

A water-cooled cylindrical copper anode 5 cm in diameter and approximately 10 cm long served as the anode. An electromagnet was used to generate a solenoidal magnetic field in the cathode region. The assembly was designed for temperature measurements of the NSTAR hollow cathode;[16] thus, the standard magnetic field current of 15A produces a magnetic field at the cathode orifice like that produced in the NSTAR thruster by the permanent magnet rings. Unless otherwise noted, the axial field strength at the cathode

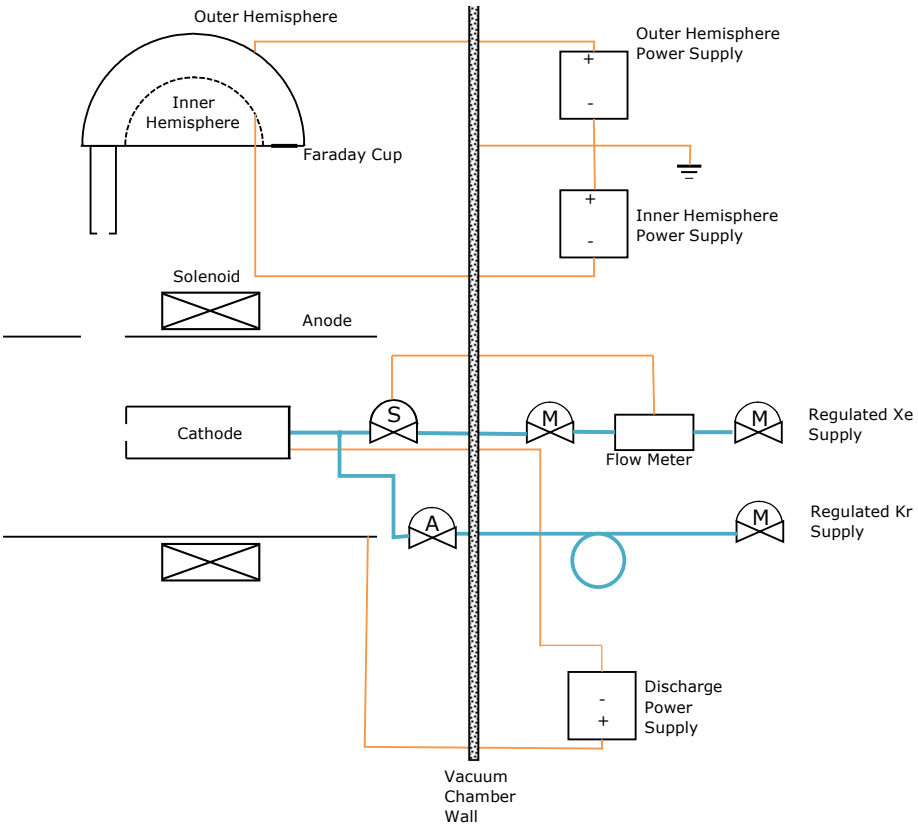

Figure 3. Schematic of the experimental setup displaying the analyzer, the cathode and anode assembly, the flow system, and electrical controls.

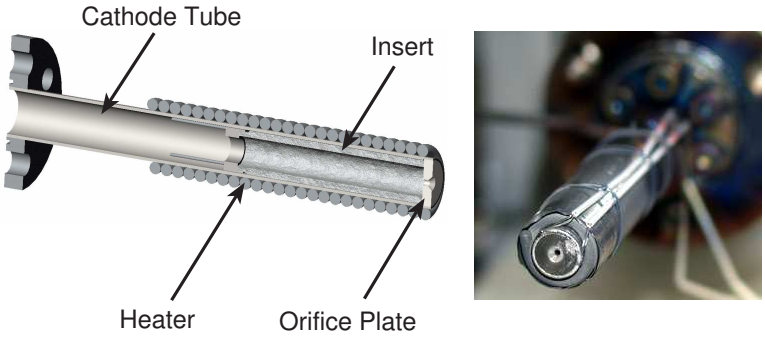

Figure 4. Cutaway diagram showing the cathode configuration and photograph of the cathode.

orifice was 82G, which corresponds to a magnetic field current of 15A. However, during the experiment the current to the solenoidal magnetic field was varied from 0A to 15A.

B. Flow System

The xenon and krypton flow systems are shown schematically in Fig. 5. The flow rate of ultra-high purity xenon (99.9995% pure) was measured with a Unit Instruments 1661 flow meter and was controlled with an MKS 250C controller and an MKS 248 valve. The meter was calibrated by flowing the respective propellants into a known volume and measuring the rate of pressure rise with a precision pressure transducer, yielding flow rate measurements with an uncertainty of less than 2%. The metering valve was mounted in the vacuum chamber so that all external feed lines were above atmosphere pressure to eliminate the possibility of air

leaks into the flow system. All feed system tubing and components had electropolished wetted surfaces and metal seals. An Optomux data system with LabView control software was used for flow setpoint control and flow meter data logging.

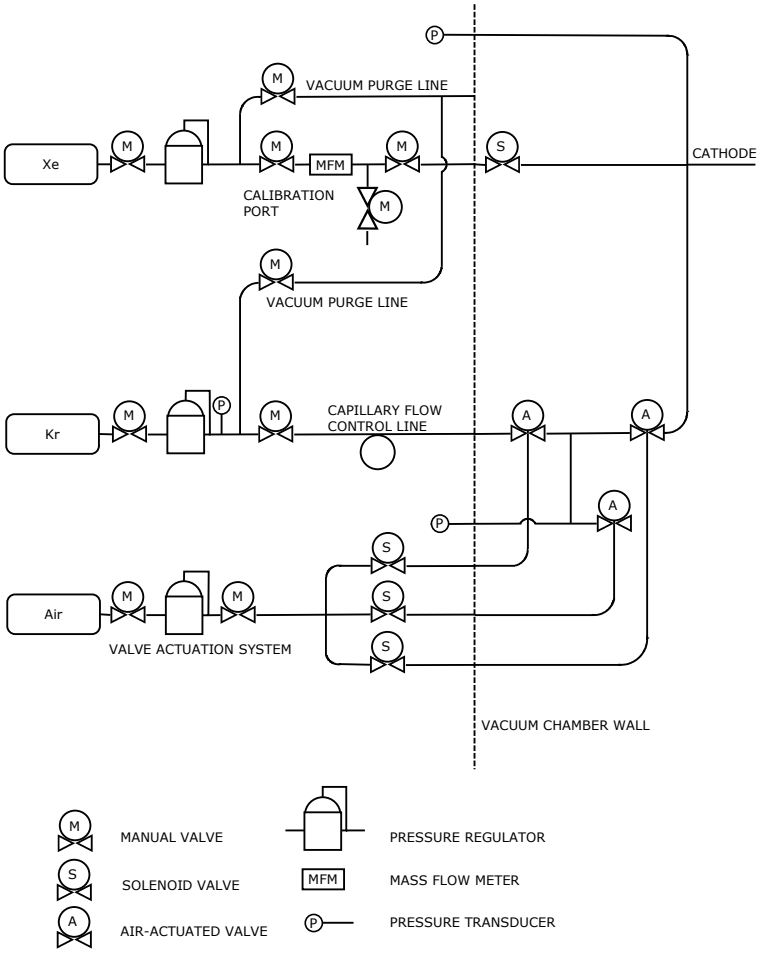

Figure 5. Schematic of the xenon and krypton flow systems.

The krypton feed system (Fig. 5) was designed to control and measure krypton flow rates up to 0.6sccm. Research grade krypton at a regulated pressure of up to 100psia was maintained in the external manifold. A pressure transducer was used to measure the manifold pressure. A 9.8m long fused silica capillary tube with an inner diameter of 100μm served as a flow restricter. Flow rate through the capillary was sensitive to gas viscosity, so the coiled tube was routed through an enclosure maintained at a constant 40°C. The flow rate as a function of upstream pressure was determined by flowing krypton into a calibrated volume and measuring the rate of pressure rise with a high accuracy pressure transducer. The calibration volume was contained inside the vacuum chamber to minimize the possibility of air leaks. The only joint in the calibration manifold was a VCR fitting on the pressure transducer which was periodically tested for leaks. Three pneumatically-actuated valves inside the vacuum chamber were used to vent the calibration volume into the vacuum chamber and to control the flow of krypton into the manifold and out of the manifold to the cathode. The calibration curve is shown in Fig. 6.

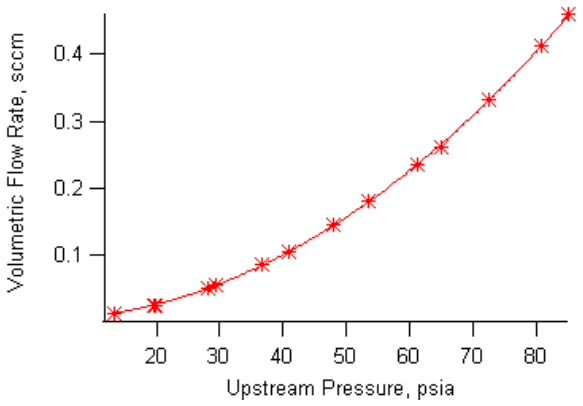

Figure 6. Calibration of the krypton flow rate through a 100μm capillary tube.

C. Electrostatic Analyzer

Electrostatic energy analyzers can have several geometries: parallel plates, cylindrical electrodes, and spherical sector electrodes. This study employs a concentric hemispherical analyzer (CHA), in which two concentric hemispheres, having different applied voltages, create a radial electrostatic field given by

$$\mathcal{E}(r) = \frac{(V_2 - V_1)R_1R_2}{(R_1 - R_2)r^2}\hat{r}, \tag{1}$$

where $\mathcal{E}$ represents the electric field, V_1 and V_2 are the voltages applied to the inner and outer hemispheres, respectively, and R_1 and R_2 are the radii of the inner and outer hemispheres, respectively. An ion entering the CHA will either impact the hemispheres or pass through along a circular orbit. If the kinetic energy with which the ion enters is such that the centrifugal acceleration balances the radial electrostatic force as in Eq. 2, the ions that pass through the hemispheres are detected by a faraday cup. This particular ion energy that produces a circular orbit is known as the transmission energy.

$$\frac{mv^2}{R_c} + q\mathcal{E}(R_c) = 0 \tag{2}$$

Substituting for the electric field and for the kinetic energy, $2E = mv^2$, and for the trajectory radius, $R_c = (R_1 + R_2)/2$ demonstrates the ESA can only filter ions based on their ratio of energy to charge. Thus, a doubly charged ion will appear the same as a singly charged ion with half of the energy.

$$\frac{E}{q} = \frac{(V_2 - V_1)R_1R_2}{(R_2^2 - R_1^2)} \tag{3}$$

The ideal resolution of a CHA is given by[17]

$$\frac{\Delta E}{E} = \frac{w}{2R_c} + \frac{(\Delta\alpha)^2}{2}, \tag{4}$$

where w is the diameter of the entrance aperture and $\Delta\alpha$ is the angular deviation from the normal to the entrance plane as illustrated in Fig. 7. Thus, for this CHA, the ideal resolution is 0.037. To improve this resolution a collimator, approximately 7cm in length with a 2.5mm diameter aperture, was added to the entrance of the CHA; however, imperfections in the fabrication of the hemispheres were the most likely source of error in the instrument resolution.

D. Test Facility

The cathode assembly was mounted in a 1m diameter by 2m long vacuum facility. This chamber was pumped by two 25cm diameter cryopumps. Pressure was monitored with a Granville Phillips Stabil Ion Gauge which was calibrated with xenon gas. The base pressure was typically 1×10^{-4}Pa (1×10^{-6}Torr) and the pressure during cathode operation was on the order of 10^{-2}Pa (10^{-5}Torr).

Heater and discharge power were provided by a Sorenson DLM 40-15 power supply and a Power Ten P62B-5060 power supply, respectively, with the common returns grounded to the vacuum tank. The cathode was also grounded to the chamber through the mounting structure. Currents and voltages were measured to within 1% by the data system using calibrated shunts and voltage dividers. A Textronix DPO 4034 oscilloscope was used to record fluctuations of the discharge voltage at 250kHz, 25MHz and 100MHz.

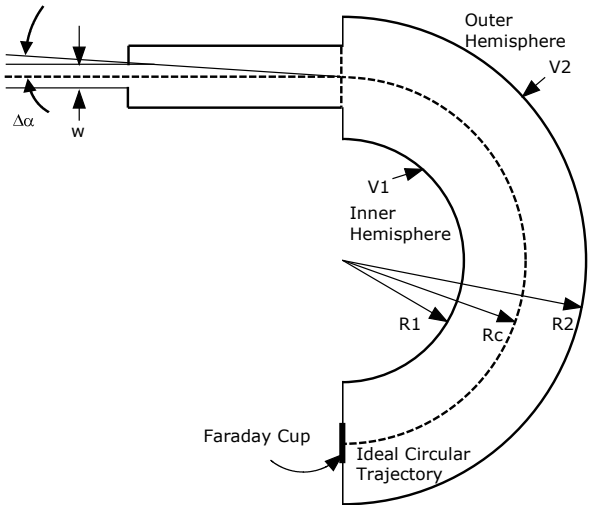

Figure 7. Schematic of the concentric hemispherical analyzer.

Inner hemisphere and outer hemisphere voltages were applied by a Kepco BOP-1M and a Sorensen DLM 150-4, respectively, with common returns grounded to the vacuum tank. For a specified transmission energy, a LabView VI controlled the applied voltages such that the centerline voltage remained at ground potential. The voltages applied to the hemispheres were within 0.2V of the specified voltage. The voltage outputs from the power supplies were measured and recorded by a data system using voltage dividers. The faraday cup current was measured with a Keithley 6485 Picoammeter to within 0.4% and recorded with the data system.

V. Procedure

Initially, the cathode was subjected to a 4 hour preheat sequence at several different current levels to condition it before operation. The cathode was typically conditioned and operated overnight after any air exposure to allow the discharge to stabilize before data acquisition. The data were gathered in a series of scans through transmission energies ranging from 0eV to 200eV in increments of 1eV. When the discharge conditions were varied between scans, the discharge was allowed to stabilize before initiating a scan, which typically took several minutes. In prior experiments, the effects of discharge current, flow rate, and strength of the applied magnetic field were examined for both pure xenon and krypton. During this phase, the cathode expellant consisted of a mixture of krypton and xenon; the percentage of krypton in the expellant was varied to examine the impact on the discharge operation and on the high-energy ion distributions. In addition, oscillations in the discharge voltage were recorded for each condition at 250kHz, 25MHz and 100MHz.

At each transmission energy, 1000 samples of the faraday cup current and of the voltages on the hemispheres were taken at 1kHz and averaged to minimize the effects of the electrostatic pickup from the discharge. There was a small, repeatable leakage current which scales with the voltage applied to the outer hemisphere. The magnitude of the leakage current was 6.5×10^{-3}nA at 200eV transmission energy and less at lower energies. In comparison, current signal peaks were on the order of 10^{-1}nA. Because this leakage current was small and repeatable, it was subtracted out of the data. The data were also corrected to account for a slight shift from ground potential along the centerline, which resulted when the applied hemisphere voltages differed slightly from the specified voltage.

Plots of cup current versus transmission energy (in eV) were generated for each scan. Since the CHA has a small angular acceptance, these distribution functions only represent ions traveling in approximately one direction, whereas typical energy distributions are defined for ions with velocities in all directions. To clarify trends in the high energy content, the total collected current and average transmission energy, given by Eq (5) and Eq (6) respectively, were calculated for each trace using the trapezoidal rule for integration.

$$I_{total} = \int f(E/q)\, d(E/q) \tag{5}$$

$$(E/q)_{avg} = \frac{\int (E/q) f(E/q)\, d(E/q)}{\int f(E/q)\, d(E/q)} \tag{6}$$

VI. Prior Results

The first stage of this study reported the high-energy ion distributions obtained with pure xenon and pure krypton expellants.[18] Fig. 8 illustrates a typical comparison between the high energy ion distributions obtained with xenon and with krypton. For the same discharge current, flow rate, and applied magnetic field, krypton produces a greater high-energy content; while the width of the distribution is not necessarily larger than the width of the xenon distribution, the peak energy and total current collected are greater. These results suggest either that the mechanism responsible for the high-energy ions is mass dependent (i.e. lighter gases achieve greater ratios of energy to charge) or that the different operational characteristics of the discharge produced higher energy ions. Most of the distributions appear to begin a few volts above the discharge voltage. Due to the positioning of the anode and the analyzer, no low-energy ions born within the anode can reach the detector.

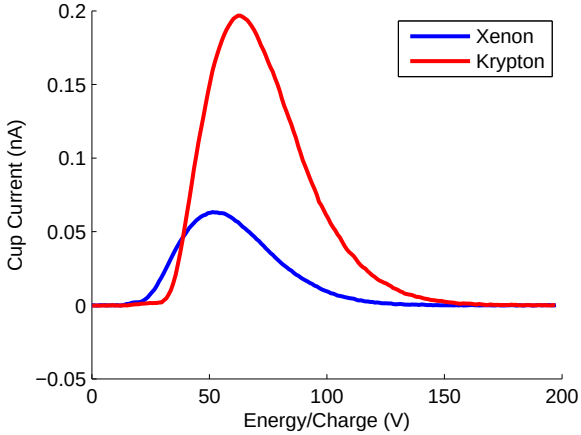

Figure 8. The comparison between high-energy content of xenon and krypton for $J_D = 18$A and $\dot{m} = 3.8$sccm (right) demonstrates the greater high-energy content obtained with krypton.

The influences of flow rate, discharge current, discharge voltage and strength of the applied magnetic field were examined. At lower flow rates, the high-energy distribution broadens and shifts to higher energies. As the discharge voltage increases, the total collected current and the average energy either increase or appear unaffected depending on the other flow conditions. While the high-energy content varies with discharge current, the character of the variation depends on other flow conditions. And finally, the applied magnetic field has a substantial impact on the high-energy content; however, its impact also depends on other flow conditions. For detailed discussion, the energy distributions, plots of total collected current, and plots of average energy at the various operating conditions, the reader is directed to the references. While no direct correlation was found between ion energy content and discharge current, discharge voltage or strength of applied magnetic field, it is possible that the mechanism for high-energy ion production scales with these parameters under certain operating conditions. Observations of plasma potentials in the cathode region indicate a change in the oscillation characteristics as the flow rate and magnetic field are varied; for example, as flow rate is reduced the oscillations transition to larger-amplitude oscillations such as those that appear in plume mode.[7] During the first phase of data collection, while the high-frequency peak-to-peak variation in the discharge voltage was not recorded, it was observed on an oscilloscope. When this peak-to-peak variation was large, there appeared to be a greater high-energy ion content. This observation is supported by the trend in high-energy content when the discharge transitions into plume mode, which is characterized by larger fluctuations in the discharge voltage.

Finally, the apparent increase in high-energy ion content, in particular, the drastic increase as the discharge enters plume mode, might have been an illusion stemming from the location of the plasma ball. In hollow cathode discharges, there is typically a bright plasma "spot" or "ball" present in front of the keeper orifice. As flow rate decreases, the plasma ball is pulled inside of the cathode, and as flow rate increases, the plasma ball moves farther out of the cathode. Similarly, as discharge current increases, the plasma ball is pulled inside of the cathode. Using high-speed scanning probes, Goebel observed large-amplitude oscillations in the plasma potential at the edge of the ball.[7] Since the CHA location was fixed, the field of view would contain different areas of the plasma ball under different conditions. In addition, since the source of the high-energy ions may be highly localized in the region of the plasma ball, it is possible that variation in the one-dimensional distributions indicate a geometric phenomenon, not a variation in the high-energy ion content.

VII. New Results

The repeatability of the cathode discharge when operated on pure xenon must be understood before the impact of krypton substitution can be characterized. Data collected on different days and at xenon flow rates of 3sccm, 4sccm and 5sccm indicate that over the range of typical operational discharge currents, the variation in the discharge voltage is up to 0.2V. More rigorous testing will be necessary to fully define the range of operation. The repeatability of the ion energy traces and the impact of variations in the discharge voltage at a set discharge current and xenon flow rate were also examined. Successive traces yield overlapping curves; however, traces collected on separate days, at the same discharge current and xenon flow rate, indicate a distinct difference in peak current collected. Therefore, the ion energy measurements are repeatable provided that the discharge plasma is unaltered; however, the inherent variability of hollow cathode operation precludes exact replication of ion energy traces. Fig. 9, which was gathered at 4sccm of xenon and 18.0A, displays a typical comparison; the energy distributions reveal a difference in peak height, which leads to a 9% increase in the total collected current.

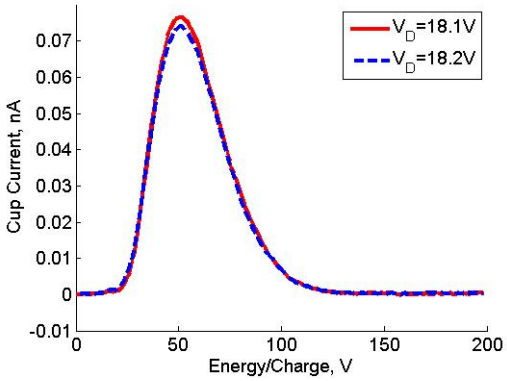

Figure 9. For a specified xenon flow rate and discharge current, both the discharge voltage and the ion-energy distributions vary. At 4sccm of xenon and 18.0A, the discharge voltage varied 0.1V when the data was gathered on separate days.

The introduction of krypton to the cathode expellant had a noticeable effect on the discharge voltage, which varied depending on the fraction of krypton in the total flow and on the other operating parameters (discharge current, total flow rate and strength of the applied magnetic field). Fig. 10 indicates that, in most cases, the addition of krypton increases the discharge voltage; however, there are a few exceptions where replacing a small fraction of xenon with krypton results in lower discharge voltage. Due to the inherent variability of the discharge plasma, additional data are necessary to define limits on the percentage of krypton which can be introduced such that the discharge operation is not altered. The lack of trends in the current data argues for further experimentation. As illustrated in Fig. 10, at a 3sccm total flow rate and a discharge current of 6.0A or 8.3A, a 5% krypton flow produces a discharge voltage closer to the discharge voltage produced with pure xenon than the discharge voltage produced with a 2% krypton flow. At a total flow rate of 3sccm, the substitution of krypton has a more noticable impact at lower discharge currents; at a total flow rate of 4sccm, the substitution of krypton has a more noticable impact at higher discharge currents; and, at a total flow rate of 5sccm, the substitution of krpyton does not appear to substantially alter the discharge voltage. Future experimentation will incorporate more rigorous data collection to define a range of discharge voltages obtained for each percentage of krypton at addtional flow rates and discharge currents.

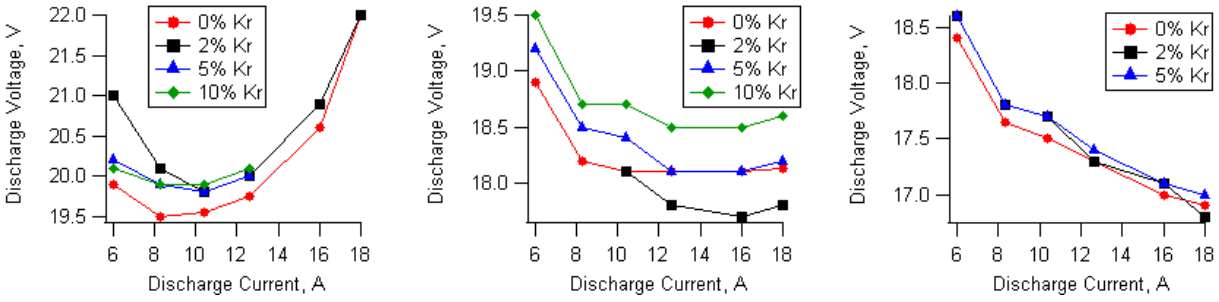

(a) Total Flow Rate = 3sccm (b) 4sccm (c) 5sccm

Figure 10. Replacing a fraction of the xenon volumetric flow rate with krypton influences the behavior of the cathode discharge. In most cases, the substitution increases the discharge voltage; however, there are a few exceptions at 2% krypton. Due to the inherent variability of the discharge plasma, additional data are needed to clearly define an upper limit on the fraction of krypton such that the discharge operation is not significantly altered.

Since 1sccm of krypton has approximately 63% of the mass of 1sccm of xenon, the sensitivity of the cathode discharge to volumetric flow rate as well as mass flow rate was examined. In these tests, the total mass flow rate, which was equivalent to the mass flow rate of 4sccm of xenon (0.393mg/s), consisted of krypton at 5% and 10% by mass; hence, the volumetric flow rate was increased. Again, the data lack consistancy. At 5% krypton, the cathode discharge appears more susceptible to changes in volumetric flow rate than to changes in mass flow rate (Fig. 11). At 10% krypton, the cathode discharge appears more susceptible to changes in mass flow rate than to changes in volumetric flow rate.

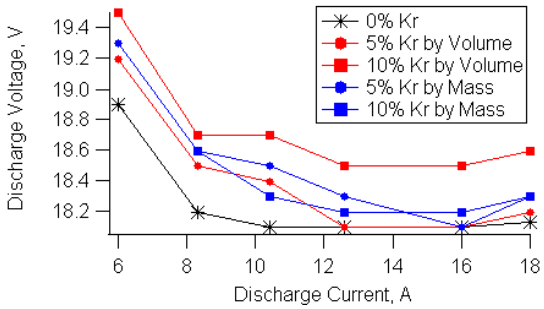

Figure 11. The cathode discharge sensitivity to volumetric flow rate and to mass flow rate is inconsistent. At 5% krypton, the cathode discharge appears more susceptible to changes in volumetric flow rate than to changes in mass flow rate. At 10% krypton, the cathode discharge appears more susceptible to changes in mass flow rate than to changes in volumetric flow rate.

Fig. 12 displays the impact of krypton on the energy distribution at a volumetric flow rate of 4sccm and of 5sccm. As the percentage of krypton increases from 0% to 5% to 10% at 4sccm, there appears to be a systematic increase in the high-energy ion content. The height of the peak, the average energy and the total collected current increase with increasing percentages of krypton. However, there is no clear trend for the 5sccm case; the peak hieght decreases slightly for 2% krypton, yet increases slightly for 5% krypton. In addition, the average energy is greatest for 2% krypton, not 5%. It is unclear whether the alteration in the high-energy ion distribution indicates preferrential acceleration of krypton or whether it reflects the different operational characteristics of the discharge.

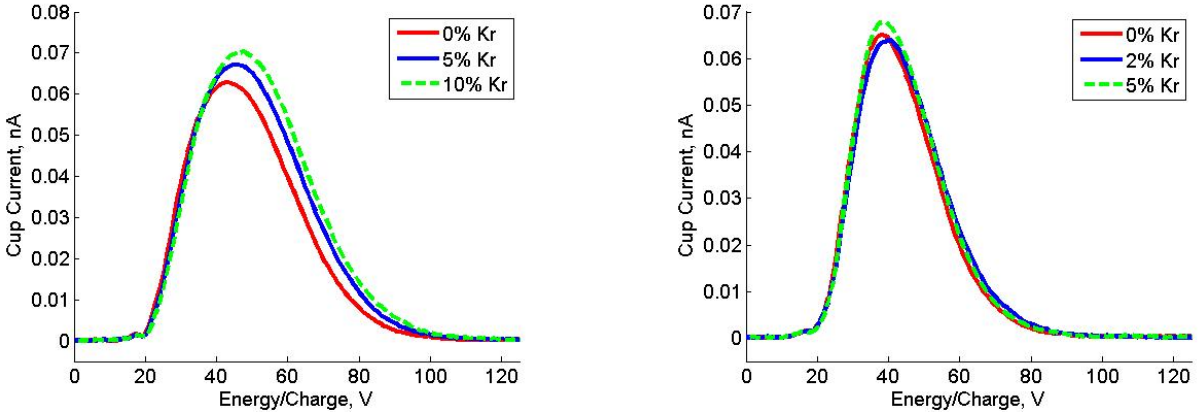

(a) Total Flow Rate = 4sccm

(b) 5sccm

Figure 12. The high-energy ion distribution responds systematically to increases in the percentage of krypton at the volumetric flow rate of 4sccm. However, the response lacks consistency at the volumetric flow rate of 5sccm, where the peak height decreases slightly for 2% krypton, yet increases slightly for 5% krypton.

While trends based on the fraction of krypton in the cathode expellant were lacking, both the total collected current and the average energy of the high-energy ion distribution scale with the peak-to-peak fluctuations in the discharge voltage (Fig. 13). Both data sets can be fit to a shifted-exponential curve of the form

$$y = y_0 + A * exp(-(x - x_0)/\tau). \tag{7}$$

For total collected current versus the peak to peak voltage fluctuation, $y_0 = 9.269 \pm 0.465$, $A = -8.5255 \pm 0.441$, $x_0 = 2.2$, and $\tau = 4.2207 \pm .454$. For the average energy versus the peak to peak voltage fluctuation, $y_0 = 101.68 \pm 3.05$, $A = -62.701 \pm 2.89$, $x_0 = 2.2$, and $\tau = 4.3471 \pm 0.416$. If the acceleration mechanism for high-energy ions were wave-based, then correlations between the amplitude of the oscillations in the discharge voltage would be expected. However, at this time, there is no theoretical explanation for the form of the obtained curve fit.

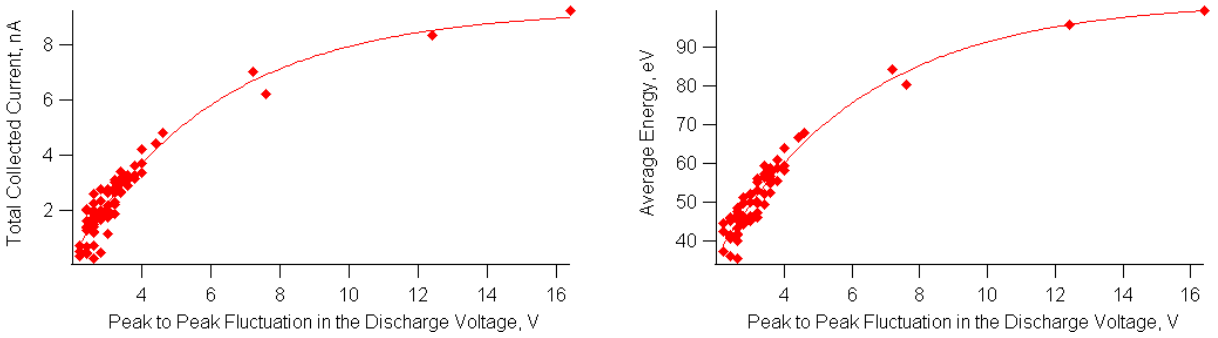

(a) (b)

Figure 13. The correlation between the total collected current and the peak to peak fluctuations in the discharge voltage, as well as the correlation between the average energy and the peak to peak fluctuation supports the statement that a wave acceleration mechanism is responsible for the high-energy ions in the discharge plasma of hollow cathodes.

Fig. 14 displays the power spectrum collected at peak-to-peak variations of 2.6V, 3.0V, and 12.4V in the discharge voltage, which correspond to average energies of 35.6V, 45.1V and 95.7V, respectively. There are oscillations up to 2MHz, twice as fast as those detected previously.[7] An increase in high-energy ion content corresponds to an increase in the amplitude of the oscillations, not an shift in the frequencies that are present. The low peak-to-peak variation (left) of 2.6V appears near the lower cut-off of peak-to-peak variations for this configuration; it occurred at a flow rate of 5sccm and at a discharge current of 8.3A. As the amplitude of the discharge voltage oscillations increases, the dominance of frequencies up to 2MHz becomes prominent. When the discharge enters plume mode, the dominance of the oscillations below 2MHz increases substantially; at a flow rate of 3sccm and a discharge current of 18A (right), the power spectrum for these frequencies is an order of magnitude greater.

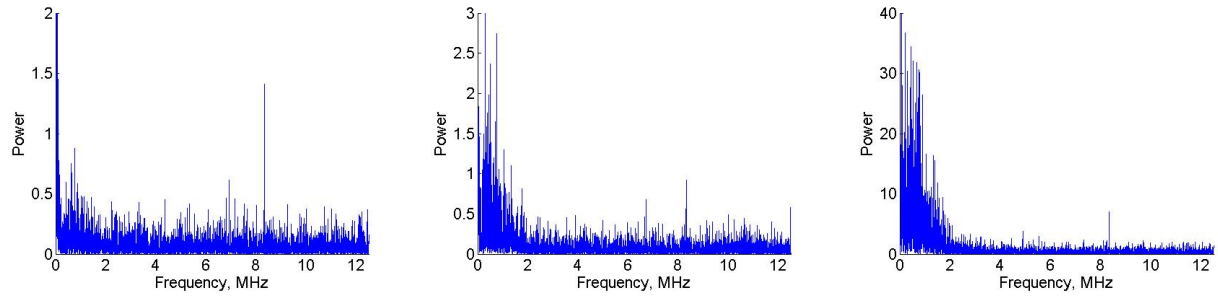

(a) 5sccm, 8.3A (b) 5sccm, 12.6A (c) 3sccm, 18.0A

Figure 14. High-frequency oscillations up to 2MHz, as displayed in power spectrum obtained at a sampling frequency of 25MHz, become more prominent as the high-energy ion content increases. The low amplitude oscillation of 2.6V in (a) is at the lower limit of peak-to-peak variations in the discharge voltage. As the amplitude increases to 3.0V (b), the dominance of frequencies up to 2MHz becomes prominent. And when the amplitude is near the maximum observed at 12.4V, which occurred when the cathode was operating in plum mode, the power of frequencies below 2MHz increases by a factor of 10.

VIII. Conclusion

As part of a larger effort to gain insight into the mechanisms responsible for producing high-energy ions in the near-plume region of hollow cathodes, this study has explored the high-energy component of the radial, quasi-one-dimensional distributions obtained using propellant mixtures of xenon and krypton. A fraction of the xenon expellant was replaced with krypton such that either the total mass flow rate or the total volumetric flow rate was conserved, and the effects on both discharge operation and on the high-energy ion content were observed. At some percentages, flow rates and discharge currents, the presence of krypton in

the propellant increased the discharge voltage; and at others, it reduced the discharge voltage. High-energy ion traces were influenced by the addition of krypton as well. At many, though not all, combinations of flow rate and discharge current, peak current and the energy at which it occurred tended to increase as the amount of krypton is increased. Unfortunately, it is unclear whether the alteration in the high-energy ion distribution indicates preferential acceleration of krypton or whether it reflects the different operational characteristics of the discharge. The variability of discharge operation and the lack of clear trends in the data argue for further experimentation; in particular, since the discharge voltage may vary by 0.2V when operated on pure xenon at a specified flow rate and discharge current, repeated testing at each condition is warranted in order to define clear bounds on performance.

The observation of ions in excess of 100eV, which was generally four times greater than the maximum of the discharge voltage, indicates that electrostatic acceleration, either through the DC potential or from the peak of the high frequency fluctuations to cathode potential, is insufficient to explain the high-energy ion content. In order to explain the observed ion energies, charge-exchange collisions must supplement electrostatic acceleration. In addition, the potential structure only supports radial acceleration of ions, which would not account for the high-energy ions measured downstream in other studies; and thus, an additional mechanism would be necessary to provide high-energy ions moving axially.

Concurrent analysis of oscillations in the discharge voltage revealed that the total current collected and the average energy of each high-energy ion distribution are functions of the peak-to-peak fluctuations in the discharge voltage. When data from multiple traces were examined, a shifted-exponential relationship was found. This correlation suggests that wave acceleration processes are a primary mechanism for high-energy ion production and radial acceleration in the discharge plasma of hollow cathodes. However, at this time, there is no theoretical model to explain the functional form. In addition, due to the complexity of non-linear wave interactions, no definitive statement can be made regarding the type of wave. Another clue was found in the frequency analysis of the discharge voltage oscillations; frequencies up to 2MHz dominated the power spectrum of the discharge voltage and became more prominent as the high-energy ion content increased.

These preliminary experiments served as a tool to guide the development of subsequent experiments. Due to the inherent variability of the discharge, future research must perform repeated analysis at each condition to carefully characterize the range of cathode operation at that condition. This extensive study will enable one to ascertain a threshold on the fraction of krypton in the propellant such that the discharge operation is not significantly altered. While neglected in this set of data, further investigations into the influence of the applied magnetic field are warranted based on prior results. To further elucidate the dependence on mass, the next stage of this study will utilize instruments capable of mass and energy analysis to examine the high-energy content when the hollow cathode is run on mixtures of xenon and krypton.

Acknowledgments

The research described in this paper was carried out at the Jet Propulsion Laboratory, California Institute of Technology. Financial support from the "GALCIT Aerospace Fund" is gratefully acknowledged.

References

[1]Sengupta, A., Brophy, J., and Goodfellow, K., "Status of the Extended Life Test of the Deep Space 1 Flight Spare Ion Engine After 30,352 Hours of Operation," 39^{th} *AIAA/ASME/SAE/ASEE Joint Propulsion Conference and Exhibit*, Huntsville, Alabama, July 2003, AIAA 2003-4558.

[2]Brophy, J. and Garner, C., "A 5,000 Hour Xenon Hollow Cathode Life Test," $27^{(th)}$ *AIAA/SAE/ASME/ASEE Joint Propulsion Conference*, Sacramento, CA, June 1991, AIAA-1991-2122.

[3]Latham, P., Pearce, A., and Bond, R., "Erosion Processes in the UK-25 Ion Thruster," 22^{nd} *International Electric Propulsion Conference*, Italy, Oct 1991.

[4]Williams, J. and Wilbur, P., "Electron Emission from a Hollow Cathode-Based Plasma Contactor," *Journal of Spacecraft and Rockets*, Vol. 29, No. 6, 1992, pp. 820–829.

[5]Farnell, C. and J.D.Williams, "Measurement of Ion Energy Distributions Produced within a NSTAR Discharge Chamber," 40^{th} *AIAA/ASMA/SAE/ASEE Joint Propulsion Conference and Exhibit*, Fort Lauderdale, Florida, July 2004, AIAA 2004-3432.

[6]Kameyama, I. and Wilbur, P., "Measurements of Ions from High-Current Hollow Cathodes Using Electrostatic Energy Analyzer," *Journal of Propulsion and Power*, Vol. 16, No. 3, May-June 2000, pp. 529–535.

[7]Goebel, D., Jameson, K., Katz, I., and Mikellides, I., "Energetic Ion Production and Keeper Erosion in Hollow Cathode Dishcharges," 29^{th} *International Electric Propulsion Conference*, Princeton, NJ, Oct-Nov 2005.

[8]Jameson, K., Goebel, D., and Watkins, R., "Hollow Cathode and Keeper-Region Plasma Measurements," 41^{st} *AIAA/ASME/SAE/ASEE Joint Propulsion Conference and Exhibit*, Tucson, Arizona, July 2005.

[9]Kolasinski, R. and Polk, J., "Characterization of Cathode Keeper Wear by Surface Layer Activation," 39^{th} *AIAA/ASME/SAE/ASEE Joint Propulsion Conference and Exhibit*, Huntsville, Alabama, July 2003, AIAA 2003-5144.

[10]Mikellides, I., Katz, I., Goebel, D., and Jameson, K., "Evidence of Nonclassical Plasma Transport in Hollow Cathodes for Electric Propulsion," *Journal of Applied Physics*, Vol. 101, No. 6, March 2007, pp. 063301.

[11]Mikellides, I., Katz, I., Goebel, D., Jameson, K., and Polk, J., "The Partially-Ionized Gas and Associated Wear in Electron Sources for Ion Propulsion, II: Discharge Hollow Cathode," 43^{rd} *AIAA/ASME/SAE/ASEE Joint Propulsion Conference and Exhibit*, Cincinnati, OH, July 2007, AIAA 2007-5192.

[12]G.J. Williams, J., Smith, T., Klick, K., Hidaka, Y., and Gallimore, A., "FMT-2 Discharge Cathode Erosion Rate Measurements via Laser-Induced Fluorescence," 36^{th} *AIAA/ASME/SAE/ASEE Joint Propulsion Conference and Exhibit*, Huntsville, Alabama, July 2000, AIAA-2000-3663.

[13]Rovey, J., Gallimore, A., and Herman, D., "Potential Structure and Propellant Flow Rate Theory for Ion Thruster Discharge Cathode Erosion," 29^{th} *International Electric Propulsion Conference*, Princeton, NJ, Oct-Nov 2005, IEPC 2005-022.

[14]Katz, I., Mikellides, I., Goebel, D., Jameson, K., Wirz, R., and Johnson, L., "Production of High Energy Ions Near an Ion Thruster Discharge Hollow Cathode," 42^{nd} *AIAA/SAE/ASME/ASEE Joint Propulsion Conference and Exhibit*, Sacramento, CA, July 2006, AIAA 2006-4485.

[15]Jahn, R., *Physics of Electric Propulsion*, McGraw-Hill Book Company, San Francisco, CA, 1968.

[16]Polk, J., Grubisic, A., Taheri, N., Goebel, D., Downey, R., and Hornbeck, S., "Emitter Temperature Distributions in the NSTAR Discharge Hollow Cathode," 41^{st} *Joint Propulsion Conference*, Tucson, AZ, 2005, AIAA-2005-4398.

[17]Moore, J., Davis, C., and Coplan, M., *Building Scientific Apparatus: A Practical Guide to Design and Construction*, Addison-Wesley, Redwood City, CA, 2nd ed., 1989.

[18]Przybylowski, J., "Dependence of the Energetic Ion Distribution on Propellant Composition in Hollow Cathodes," 43^{rd} *Joint Propulsion Conference*, Cincinnati, OH, 2007.